Suppression of Sub-Synchronous Resonances through Excitation Control of Doubly-Fed Induction Generators

Hana Jannaty Baesmat, *Student Member, IEEE*, Marc Bodson, *Fellow, IEEE*

Abstract— **The paper considers the problem of sub-synchronous resonances (SSR) in doubly-fed induction generators connected to the grid through series-compensated lines. The existence of oscillations is observed on a laboratory test-bed in various conditions, with instabilities developing in the worst-case scenario. Despite the limitations of a small-scale test-bed, the ability to investigate problems and solutions in ways that would not be possible on a full-scale system is very valuable. In particular, the paper demonstrates the significant effect of the choice of dq reference frame on the severity of SSR. Stator-aligned algorithms are found to be significantly more resonant than grid-oriented algorithms, as evidenced in experiments as well as using an analysis method proposed in the paper. From this observation, an algorithm is proposed to emulate a grid-alignment using stator voltages and currents, but without measurements of the grid and series-capacitor voltages. Two control laws are then presented to regulate the active and reactive powers generated, resulting in well-damped transient responses. SSR oscillations are found to be eliminated in experiments, as well as simulations of a full-scale system and using a frequency response analysis of the closed-loop system. The effectiveness of the proposed control schemes is verified through experiments for different compensation levels and varying speeds. Within the assumptions made in the design, the proposed controllers are global.**

Index Terms— Doubly-fed induction generators (DFIG), complex domain, pole-placement controller, LQR controller, reference frame alignment, dq coordinates, observer.

I. INTRODUCTION

THE steady growth of wind power generation has led to the development of more efficient wind turbines. Variable-speed wind turbines have shown to increase the energy generation anywhere from 3 to 28 percent and exhibit superior power quality compared to the simple fixed-speed wind turbines [1]. Therefore, they are now considered the most common type of installed turbines [2]. Amongst the variable-speed generators, doubly-fed induction generators (DFIG) have gained significant attention due to their power electronic converter being rated at only 25%-30% of the generator nameplate power [3]; this results in reduced power losses as well as lower converter costs [1].

The stator of a DFIG is connected directly to the grid while its rotor winding is connected via a back-to-back AC/DC/AC power converter. The AC/DC converter, referred to as the rotor side converter (RSC), controls the active and reactive powers at the stator terminals while the DC/AC converter, referred to as the grid side converter (GSC), aims to maintain a constant voltage on the DC link capacitor between the converters [4].

With wind farms often located in remote areas where the wind speeds are favorable, long transmission lines are needed to transfer the generated power to load centers [5]. Therefore, most of these transmission lines are series-compensated to allow for increased transmission capacity and reduced voltage drops. However, the interaction of energy between the DFIG and the series-compensated line sometimes introduces a sub-synchronous resonance (SSR) phenomenon that can create electrical instabilities at frequencies below the nominal system frequency and lead to failure of turbine-generator shafts [6-7]. Hence, the repercussions of series-capacitor compensated lines connecting DFIG wind farms to the grid must be carefully studied and analyzed.

There are three main classifications for SSR's, namely: Induction Generator Effect (IGE), Torsional Interaction (TI), and Torque Amplification (TA) [8]. While IGE is a purely electrical phenomenon, TI occurs as a result of energy exchange between the mechanical system (generator shaft) and the series-compensated line [9]. Significant system disturbances may cause the resulting electromagnetic torque to oscillate at a frequency close to the complement of one of the torsional natural frequencies, leading to resonance between electrical and mechanical natural frequencies; this is referred to as TA [10].

Several approaches have been proposed to analyze the SSR in the literature amongst which Eigenvalue Analysis, Impedance-based Analysis, and Modal Analysis are the most common. In [11], the mathematical model of the DFIG-based wind farm interconnected with a series-compensated transmission line is derived, and its stability properties are explored. The nonlinear mathematical model of the system is linearized to evaluate the system stability and sensitivity to parameter variations based on eigenvalues and a participation-factor analysis. The paper suggests that the parameters of the rotor-side current-control scheme considerably impact system stability.

In [12], the effects of series compensation, wind speed, and current loop gains are studied on IGE and TI. Eigenvalue analysis and time-domain simulations are used to evaluate the damping and torsional modes of the network. It is shown that TI only occurs for unusually high values of the shaft stiffness and compensation level, and IGE is the major source of SSR.

The authors are with the Electrical and Computer Engineering Department, University of Utah, Salt Lake City, UT 84112, USA (e-mail: hana.baesmat@utah.edu; bodson@eng.utah.edu).

Moreover, it is found that, unlike fixed speed systems, damping of the network mode that influences IGE is enhanced for higher wind speed conditions.

In [13], modal analysis of a DFIG wind farm interfaced with a series-compensated network is used to identify system modes and their characteristics. The effects of varying wind speed and converter control parameters on system modes are investigated, and time-domain simulation is performed to verify the analysis. It is shown that the dominating system modes change with varying wind speed conditions. The impact of RSC control on SSR is also explored, and the results suggest that, with the torque feedback loop open, an increasing gain can lead to the instability of the SSR mode.

The ability of the DFIG power converters in mitigating SSR is explored in [14]. An auxiliary SSR Damping Controller (SSRDC) scheme using the GSC is proposed for SSR mitigation. Residue-based analysis, root locus diagrams, and time-domain simulation verifications are used to select effective control signals. It is found that the capacitor voltage is an effective signal in increasing SSR damping. A similar approach is taken in [15] to design an SSRDC with an optimum input control signal using residue-based analysis and root-locus method. The effectiveness of the selected control signal is measured by its ability to stabilize the SSR mode without destabilizing other modes of the system.

In [6], an improved impedance model-based method using aggregated *RLC* circuit model is proposed to analyze the characteristics of SSR. The proposed scheme allows a quantitative evaluation of SSR stability through circuit parameters. The contribution of the GSC, DC link, the outer control loop of RSC, and the number of online DFIGs to SSR is also investigated. A supplementary damping control scheme is developed in [16] that employs a multi-input-multi-output (MIMO) state-space approach to mitigate SSR. Both GSC and RSC control loops are analyzed and compared; the results of the comparison show that RSC damping control exhibits superior damping, lower actuator control effort, and higher robustness under changing operating conditions.

In [17], the dynamic phasor-based modeling approach is used to develop the impedance model of a thyristor-controlled series capacitor (TCSC), and the application of the derived impedance model in Type-3 wind energy systems for SSR is investigated. The paper shows that the TCSC is successful in avoiding SSR in DFIG wind farms. Moreover, it is found that RSC current control does not lead to SSR instability.

Modal analysis and time-domain simulations are used in [18] to show that the fixed capacitor-compensated DFIG farm is highly unstable in the SSR mode. Residue-based analysis and root-locus diagrams are then used to design an SSRDC for the DFIG-based wind farm compensated with Gate-Controlled Series Capacitor (GCSC).

Two major approaches are used for mitigating SSR in the literature. The first approach uses Flexible Alternating Current Transmission System (FACTS) devices [17-20], and the second uses DFIG controllers [6], [11-16]. This paper falls into the second category. A distinct feature of the paper compared to other references in the literature is the experimentation with a real system, as opposed to simulations. Such experiments would be difficult, if not impossible, to perform on a full-size generator connected to the grid. The use of a laboratory test-bed has its limitations but includes many real-life effects that are not modeled in simulation studies. In this manner, the results of this paper complement the aforementioned literature on SSR and provide some new information. Although previous works [11-12], [15-16], show that the RSC control loop negatively affects SSR, it is shown in this paper that the alignment of the reference frame for dq transformation has a significant effect on IGE. With proper alignment of the reference frame and design of the control system, the RSC becomes a stabilizer of SSR, much as a power system stabilizer dampens oscillations in synchronous generators. The method does not require the use of costly FACT devices to avoid SSR. The effectiveness of the proposed approach at different compensation levels and multiple speeds is demonstrated through experiments on a laboratory test-bed as well as simulations on a full-scale system. Analysis methods are also proposed to compute the frequency response of the open-loop and closed-loop systems.

Oscillations can also appear in the tie-lines between multiple wind farms and the rest of a power system [21], in particular above a certain level of penetration. However, this paper focuses on mitigating resonances caused by the interaction between a single wind turbine or wind farm and a series-compensated transmission line.

The main contributions of the paper are outlined below:
1. The observation of SSR effects in a DFIG test-bed with the series-compensated line (very little experimental data can be found in the literature on this subject).
2. The demonstration of the significant effect of reference frame alignment on SSR, and an analysis method that predicts and explains the poor damping with the stator-aligned reference frame.
3. The development of two RSC control laws to mitigate SSR oscillations without the need for costly FACT devices or auxiliary sub-synchronous damping controllers. Unlike other schemes in the literature that provide a lightly damped response, the controllers of this paper eliminate the SSR oscillations and show convergence in the same time span as a system without a series-compensated line.
4. The design and analysis of the proposed controllers directly in the complex domain. This allows the reduction of the order of the system, including the controller gains, by a factor of 2.
5. Validation of the effectiveness of the proposed controllers through experiments, frequency-domain analysis, and simulations on a full-scale wind farm in Simscape/MATLAB.

II. SERIES-COMPENSATED DFIG IN DQ COORDINATES

Fig. 1 shows the basic elements of a DFIG connected to the grid through a series-compensated line. The prime mover is typically a wind turbine, and the rotor-side-converter (RSC) controls the amount of power transferred to the grid through the stator. A transmission line in series with a capacitor (both three-
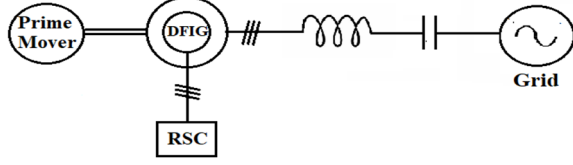
phase) connects the stator to the grid.

Fig. 1. DFIG connected to the grid through a series-compensated line

The dynamic model of a DFIG with a series-compensated line is given by the following equations in dq coordinates:

$$(L_s + L_l)\frac{di_{sd}}{dt} + M\frac{di_{rd}}{dt} = v_{gd} - v_{cd} - (R_s+R_l)i_{sd} +$$
$$\omega_e\left((L_s + L_l)i_{sq} + Mi_{rq}\right) \tag{1}$$

$$(L_s + L_l)\frac{di_{sq}}{dt} + M\frac{di_{rq}}{dt} = v_{gq} - v_{cq} - (R_s+R_l)i_{sq} -$$
$$\omega_e\left((L_s + L_l)i_{sd} + Mi_{rd}\right) \tag{2}$$

$$L_r\frac{d\,i_{rd}}{dt} + M\frac{di_{sd}}{dt} = v_{rd} - R_r i_{rd} + \omega_s\left(L_r i_{rq} + Mi_{sq}\right) \tag{3}$$

$$L_r\frac{di_{rq}}{dt} + M\frac{di_{sq}}{dt} = v_{rq} - R_r i_{rq} - \omega_s\left(L_r i_{rd} + Mi_{sd}\right) \tag{4}$$

$$c\frac{dv_{cd}}{dt} = i_{sd} + c\omega_e v_{cq} \tag{5}$$

$$c\frac{dv_{cq}}{dt} = i_{sq} - c\omega_e v_{cd} \tag{6}$$

with the following definitions:

$i_{sd}, i_{sq}, i_{rd}, i_{rq}$: direct and quadrature components of the stator and rotor currents, respectively

$v_{sd}, v_{sq}, v_{rd}, v_{rq}$: direct and quadrature components of the stator and rotor voltages, respectively

$v_{cd}, v_{cq}, v_{gd}, v_{gq}$: direct and quadrature components of the capacitor and grid voltages, respectively

L_s and L_r: stator and rotor inductances, respectively

M: mutual inductance between the stator and the rotor

R_l and L_l: line resistance and inductance, respectively

R_s and R_r: stator and rotor resistances, respectively

ω_e: the angular electrical frequency of the rotating dq frame of reference (normally equal to the frequency of the grid)

ω: mechanical speed

$\omega_s = (\omega_e - n_p\omega)$: slip frequency

n_p: number of pole pairs

c: series capacitance

Series compensation refers to the placement of capacitors in series with the transmission line to compensate for the line's inductive reactance. The benefits are enhanced power flow capabilities and improved voltage regulation. The level of compensation of a series-compensated line in a DFIG system plays a significant role in the stability of the system. The higher the compensation level, the more the system is prone to instability [22]. Therefore, to validate the effectiveness of the proposed SSR mitigation techniques, two compensation levels were studied: 50% and 70%. This paper only reports the results for a 70% compensation level. An n% compensation level indicates that the reactance of the capacitor compensates for n% of the transmission line reactance. Specifically, for a 60 Hz

distribution system:

$$c = \frac{1}{nL_l(2\pi\,60)^2} \tag{7}$$

Note that 100% compensation results in an LC network with a resonance at 60 Hz, which is problematic.

III. PRELIMINARY ANALYSIS

In this section, the results of SSR experiments performed on the laboratory test-bed are presented. Two cases are considered for control. In the first case, steps of v_{rd}, v_{rq} are applied to the system. We refer to this case as open-loop dq control. In the second case, an integral controller is added to track references of active and reactive power. We refer to this case as closed-loop dq control. Also, in both cases, two approaches are considered for dq orientation. The first approach derives the angle for the dq transformation from the stator voltages and is such that $v_{sq} = 0$. This approach is referred to as the stator alignment. The second approach is based on the grid voltages and is such that $v_{gq} = 0$. This approach is referred to as the grid alignment. Note that the second approach is not quite practical in a power system since it requires a measurement of the grid voltages at a high sampling rate for the implementation of the control system and this measurement is to be taken at a distant location from the generator. Nevertheless, the conclusions are significant in understanding SSR and deriving solutions to the problem.

A. Open-loop system

The active and reactive powers generated by the DFIG are shown in Fig. 2 for the open-loop control case. On Fig. 2, the results with grid and stator alignments are shown, as well as the results without the series-compensated line for comparison (in that case, the stator voltages and the grid voltages are the same). Steps of v_{rq} are applied first (which mostly impacts active power), followed by steps of v_{rd} (which mostly impacts reactive power). An important observation is that oscillations are much more significant with the stator alignment approach. With a 70% compensation level, the system with stator alignment almost becomes unstable. A conclusion to be drawn is that it is not so much the presence of the series-compensated line that causes the SSR problem, but the presence of the line in combination with the stator alignment.
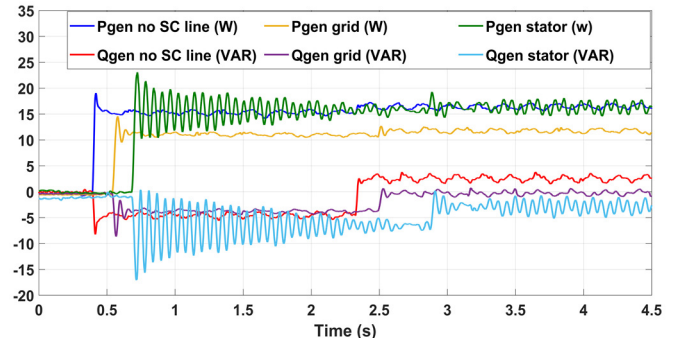

Fig. 2. Grid vs stator alignment for an open-loop controller and 70 percent compensation

B. Closed-loop system

The SSR phenomenon is further demonstrated in the closed-loop control case on Fig. 3. The problem is found to be severely magnified by the additional feedback. With 50% compensation (results not reported in the paper), the SSR manifests itself as sustained oscillations. With 70% compensation, the stator alignment approach leads to instability, with the protection of the power electronics drive board tripping. Again, the problem is greatly reduced with grid alignment.
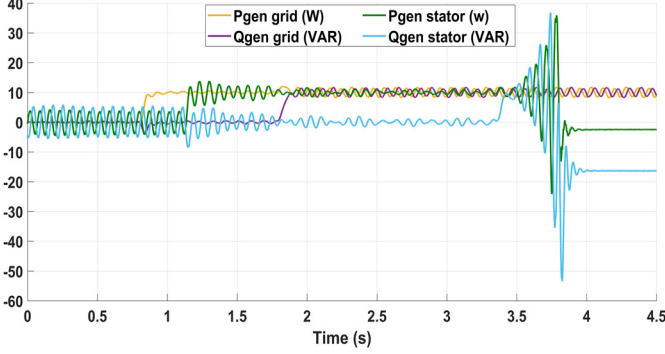

Fig. 3. Grid vs. stator alignment for a closed-loop controller and 70 percent compensation

IV. ANALYSIS OF STABILITY WITH GRID AND STATOR ALIGNMENTS

In this section, a method of analysis is presented to explain the experimental results. In the grid alignment approach, the electrical dynamics of the system can be analyzed using (1)-(6), which can be expressed in the state-space form

$$E\dot{x} = Fx + G_1 u + G_2 d \qquad (8)$$

for some matrices E, F, G_1, G_2 and

$$x = [i_{sd} \ i_{sq} \ i_{rd} \ i_{rq} \ v_{cd} \ v_{cq}]^T, u = \begin{bmatrix} v_{rd} \\ v_{rq} \end{bmatrix}, d = \begin{bmatrix} v_{gd} \\ v_{gq} \end{bmatrix} \quad (9)$$

At constant speed and electrical frequency, the description is a linear time-invariant system. The grid voltage is an external signal with v_{gd} constant and $v_{gq} = 0$. Let

$$C = \begin{bmatrix} 1 & 0 & 0 & 0 & 0 & 0 \\ 0 & 1 & 0 & 0 & 0 & 0 \end{bmatrix} \text{ and } r = \begin{bmatrix} v_{rd,com} \\ v_{rq,com} \end{bmatrix} \quad (10)$$

where $v_{rd,com}$ and $v_{rq,com}$ are rotor voltage commands such that $u=r$ in the open-loop command case. Then, the transfer function matrix H such that

$$\begin{bmatrix} i_{sd} \\ i_{sq} \end{bmatrix} = H \begin{bmatrix} v_{rd,com} \\ v_{rq,com} \end{bmatrix} \qquad (11)$$

is given by

$$H(s) = C(Es - F)^{-1} G_1 \qquad (12)$$

In the stator alignment approach, two methods of analysis are

possible. If the stator alignment is used for analysis, one still has $v_{rd} = v_{rd,com}$ and $v_{rq} = v_{rq,com}$. However, the voltages v_{gd} and v_{gq} become functions of the stator voltages and the reference frame frequency ω_e becomes variable. This method is difficult to pursue. On the other hand, if the grid alignment is used for analysis, the frequency $\omega_e = \omega_g$ is constant, v_{gd} is constant, and $v_{gq} = 0$. However, one must compute the voltages v_{rd}, v_{rq} in the grid alignment that correspond to the voltages $v_{rd,com}$, $v_{rq,com}$ that are applied in the stator alignment. This method is more tractable.

In the grid voltage reference frame, a rotor voltage command computed in the stator reference frame is a vector $\overrightarrow{v_r}$ that is equal to the unit vector $\frac{\overrightarrow{v_s}}{|\overrightarrow{v_s}|}$ multiplied by $v_{rd,com}$, plus the same unit vector rotated by 90 degrees and multiplied by $v_{rq,com}$. Algebraically, the result is:

$$v_{rd} = \frac{v_{rd,com} v_{sd}}{\sqrt{vsd^2 + vsq^2}} - \frac{v_{rq,com} v_{sq}}{\sqrt{vsd^2 + vsq^2}}$$

$$v_{rq} = \frac{v_{rd,com} v_{sq}}{\sqrt{vsd^2 + vsq^2}} + \frac{v_{rq,com} v_{sd}}{\sqrt{vsd^2 + vsq^2}} \qquad (13)$$

The rotor voltages depend on the stator voltages, which can be obtained from:

$$L_l \frac{di_{sd}}{dt} = v_{gd} - v_{cd} - v_{sd} - R_l i_{sd} + \omega_e L_l i_{sq}$$

$$L_l \frac{di_{sq}}{dt} = v_{gq} - v_{cq} - v_{sq} - R_l i_{sq} - \omega_e L_l i_{sd} \qquad (14)$$

Equations (13) and (14) define a rotor voltage vector of the form

$$u = L(r, x, \dot{x}) \qquad (15)$$

where $L(r, x, \dot{x})$ is a nonlinear vector function of r, x, and $\dot{x}$. This equation reveals that an open-loop control method based on stator alignment is in fact a complicated nonlinear feedback system. The significant change of dynamics observed when switching from grid alignment to stator alignment is due to this feedback.

To proceed with the analysis, a possibility is to linearize (13), (14), so that (15) becomes

$$u = L_1 r + L_2 x + L_3 \dot{x} \qquad (16)$$

where L_1, L_2, L_3, are matrices that depend on the steady-state operating point. Analytic expressions for the matrices are not given, because they are complicated, and the computations of this paper were performed using the *symbolic toolbox* of *Matlab*. The result is that (8) is replaced by

$$(E - G_1 L_3)\dot{x} = (F + G_1 L_2)x + G_1 L_1 r + G_2 d \qquad (17)$$

and

$$H(s) = C\big((E - G_1 L_3)s - (F + G_1 L_2)\big)^{-1} G_1 L_1 \qquad (18)$$

The norm of the matrix H is plotted for both scenarios in Fig. 4. As can be seen from the figure, the SSR frequency is about 44 Hz in both cases. The system gain at the SSR frequency is about 15dB higher for a stator-aligned system than for the grid-aligned system. The inherent feedback embedded in the stator alignment considerably degrades the stability of the open-loop system, which also impacts the closed-loop system response. Using a grid alignment greatly simplifies any outer loop feedback design.
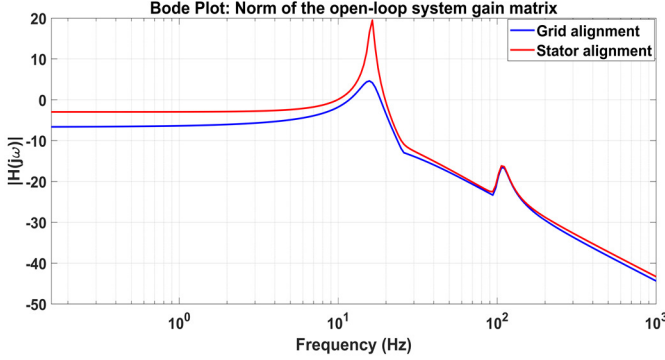

Fig. 4. The norm of the open-loop system gain for grid and stator alignment

The eigenvalue plots of both the grid and stator aligned state-space systems are presented in Fig. 5. As can be seen from this figure, the stator-aligned system has poles that are much closer to the $j\omega$ axis.
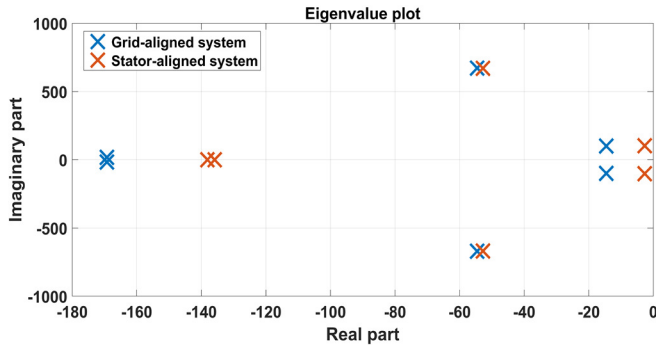

Fig. 5. Eigenvalues of the grid and stator aligned open-loop systems

Based on these observations, the control methods proposed in this paper proceed with the following principles:

- a grid-aligned reference frame is reconstructed without using grid voltage measurements
- the grid-aligned model is used to develop an observer and a feedback system to control the active and reactive powers produced.

A further element of the solution is the grouping of each pair of d and q components into a single complex variable, which simplifies the derivation and the presentation of the results.

V. COMPLEX REPRESENTATION

The application of design methods in the complex domain is based on a symmetry condition on the system that allows the reduction of the order of the system by a factor of 2, as outlined in [23]. The DFIG with series-compensated line satisfies these symmetry requirements and can be reduced from the 6th order system (1)-(6) to a 3rd order system. Complex variables are defined by $i_s = i_{sd} + ji_{sq}, i_r = i_{rd} + ji_{rq}, v_s = v_{sd} + jv_{sq}, v_r = v_{rd} + jv_{rq}, v_g = v_{gd} + jv_{gq},$ and $v_c = v_{cd} + jv_{cq}$. In this representation, the equations of the system become:

$$(L_s + L_l)\frac{di_s}{dt} + M\frac{di_r}{dt} = v_g - v_c - (R_s + R_l)i_s - j\omega_e\big((L_s + L_l)i_s + Mi_r\big) \tag{19}$$

$$L_r\frac{di_r}{dt} + M\frac{di_s}{dt} = v_r - R_ri_r - j\omega_s(L_ri_r + Mi_s) \tag{20}$$

$$c\frac{dv_c}{dt} = i_s - jc\omega_e v_c \tag{21}$$

The transformation from (line-neutral) stator voltages v_{sa}, v_{sb}, v_{sc} to the complex voltage v_s has the simple expression [24]

$$v_s = \sqrt{2/3}\, e^{-j\theta_e}\left(v_{sa} + e^{-j\frac{2\pi}{3}}v_{sb} + e^{j\frac{2\pi}{3}}v_{sc}\right) \tag{22}$$

where θ_e is the angle used for reference frame alignment and the coefficient $\sqrt{2/3}$ corresponds to the choice of a power-preserving transformation. The complex stator current is similarly defined. For the rotor voltages, a complex rotor voltage is defined by

$$v_r = \sqrt{2/3}e^{-j\theta_s}\left(v_{ra} + e^{-j\frac{2\pi}{3}}v_{rb} + e^{j\frac{2\pi}{3}}v_{rc}\right) \tag{23}$$

where $\theta_s = \theta_e - n_p\theta$ and θ is the rotor angle. The complex rotor current is similarly defined.

VI. GRID ANGLE ESTIMATION

For grid alignment, the angle θ_e is chosen such that v_g is real. However, the grid voltages are not assumed to be measured. So, the methods of this paper proceed along the following steps:

1. An angle θ_n is obtained by integrating ω_n, where ω_n is the nominal grid frequency (120π rad/s).
2. The stator voltages and currents are transformed to the complex representation using the angle θ_n.
3. The variables v_{sn} and i_{sn} are used in an observer to obtain estimates v_{go} and v_{co} of v_g and v_c. The observer also produces its own (filtered) estimate i_{so} of the stator current.
4. The angle of the grid voltage θ_o is determined from the estimate of v_{go} and the angle is subtracted from all the complex variables. As a result, v_g becomes real, and the effective reference frame alignment is $\theta_e = \theta_n + \theta_o$.

The motivation for this multi-step procedure is that a low-bandwidth observer can be designed in the intermediate frame of reference at a frequency ω_n. On the other hand, the correction θ_o ensures that steady-state corresponds to constant complex variables, even if the grid frequency is different from 60 Hz and changes slowly. The true grid frequency can be estimated from $\omega_e = \omega_n + \omega_o$, where $\omega_o = \frac{d\theta_o}{dt}$. However, that correction term being small was not applied and ω_n was used

in place of ω_e.

VII. OBSERVER

Based on (1)-(6) and (14), the following observer is proposed:

$$\begin{bmatrix} di_{so}/dt \\ dv_{co}/dt \\ dv_{go}/dt \end{bmatrix} = \begin{bmatrix} -j\omega_n - R_l/L_l & -1/L_l & 1/L_l \\ 1/c & -j\omega_n & 0 \\ 0 & 0 & 0 \end{bmatrix} \begin{bmatrix} i_{so} \\ v_{co} \\ v_{go} \end{bmatrix} + \begin{bmatrix} -1/L_l \\ 0 \\ 0 \end{bmatrix} v_{sn} + G(i_{sn} - i_{so}) \tag{24}$$

where G is a 3x1 vector chosen to yield a stable observer with fast response. In the experiments, the gains were computed so that the observer poles were placed at -600, -601, and -603 rad/s.

Fig. 6 verifies experimentally the accuracy of the observer in estimating the dq capacitor voltages for a 70% compensation scenario. Fig. 7 shows the effectiveness of the observer in reconstructing the grid voltages in the physical *abc* reference frame.
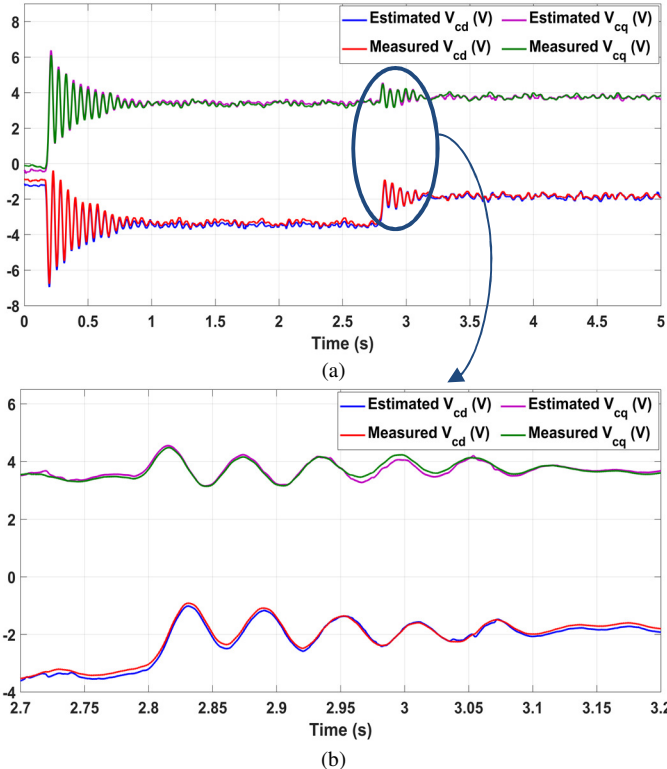

(a)

(b)

Fig. 6. Measured vs. estimated values of the capacitor voltages in the dq reference frame
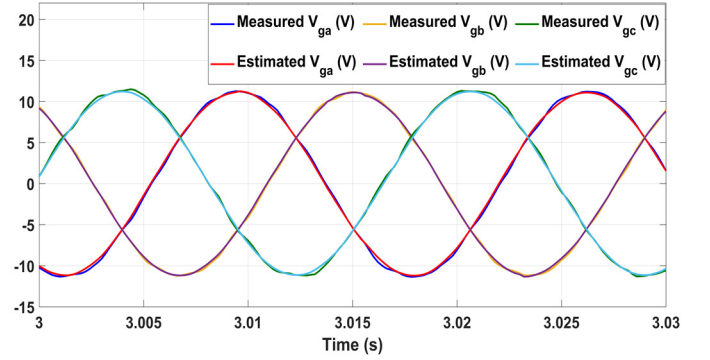

Fig. 7. Measured vs. estimated values of the grid voltages

VIII. DESIGN OF THE RSC COMPLEX CONTROL LAWS

When modeling the DFIG for SSR analysis, the parameters of the AC/DC/AC converter controllers are of interest. Between the GSC and RSC converter controllers of the DFIG, the RSC controller has been shown to have the largest impact on the SSR mode and, therefore, on the system stability. By contrast, the GSC controller does not participate significantly in the SSR mode. This has been studied extensively in the literature, and the results are reported in [7], [12]-[14]. Therefore, the controllers proposed in this paper, directly aim at the root of the problem and use the RSC only to mitigate the SSR oscillations.

In [24], [25], pole placement controllers were developed in the complex domain for a grid-connected DFIG. The algorithms were shown successful at controlling the DFIG with a direct grid connection. In the presence of a series-compensated line, however, the responses of the system with the controllers of [24]-[25] were found to be oscillatory. This paper shows how different controllers can be designed, still in the complex domain, to restore the performance and damping of the previous controllers. Two control laws are presented that use the capacitor voltages as well as the stator and rotor currents in their feedback loop. The capacitor voltages are estimated using the observer proposed in section VII, as well as the angle for the dq transformation. The complex domain framework is used as a tool to develop controllers. Real-time coding is also performed in the complex domain but translated into the real domain at the interfaces with the physical system.

A. Pole-placement controller

The pole placement control law under consideration is given by

$$v_r = R_r i_r + j\omega_s (L_r i_r + M i_s) + K_p \big(K_f\, i_{s,ref} - i_s \big) + \frac{K_i}{s} \big(i_{s,ref} - i_s \big) - K_r i_r - K_c v_c \tag{25}$$

The first two terms on the right-hand side cancel the open-loop dynamics of the system (in particular, the speed-dependent terms). The remaining terms are state feedback terms, where the state is augmented by an integrator $(i_{s,ref} - i_s)$ to achieve a zero steady-state error. Four complex feedback gains K_p, K_i, K_r, and K_c must be adjusted to ensure a stable feedback system. One feedforward gain K_f is used to adjust the zero introduced

by the controller in the closed-loop transfer function.

The process of deriving the control law and calculating the complex feedback gains in equation (25) can be summarized as follows. The state-space model of the open-loop system can be obtained from equations (19)-(21), together with

$$L_r \frac{di_r}{dt} + M \frac{di_s}{dt} = v_r \tag{26}$$

$$dx_i/_{dt} = (i_s - i_{s,ref}) \tag{27}$$

where x_i is an added state due to the integrator of the control law. It follows that the state-space model is given by

$$E = \begin{bmatrix} L_t & M & 0 & 0 \\ M & L_r & 0 & 0 \\ 0 & 0 & 1 & 0 \\ 0 & 0 & 0 & c \end{bmatrix}$$

$$F = \begin{bmatrix} -(R_t + j\omega_e L_t) & -j\omega_e M & 0 & -1 \\ 0 & 0 & 0 & 0 \\ 1 & 0 & 0 & 0 \\ 1 & 0 & 0 & -jc\omega_e \end{bmatrix}$$

$$A = E^{-1}F, \qquad B = E^{-1}[0 \ \ 1 \ \ 0 \ \ 0]^T$$

$$x = [i_s \ \ i_r \ \ x_i \ \ v_c]^T, u = v_r \tag{28}$$

where $R_t = (R_s + R_l)$ and $L_t = (L_s + L_l)$.

To place the closed-loop poles of this system at desired locations in the left half-plane (LHP), a vector of complex gains k is defined such that

$$v_r = -k(x - x_d) \tag{29}$$

where x_d is a vector of references, $x_d = [K_f \ i_{s,ref} \ 0 \ 0 \ 0]^T$, and $k = [K_p \ K_r \ K_i \ K_c]^T$

By plugging equation (29) in the open-loop state-space model of (28), the following closed-loop state-space matrix is obtained:

$$A_{cl} = E^{-1} \begin{bmatrix} -(R_t + j\omega_e L_t) & -j\omega_e M & 0 & -1 \\ -K_p & -K_r & -K_i & -K_c \\ 1 & 0 & 0 & 0 \\ 1 & 0 & 0 & -jc\omega_e \end{bmatrix} \tag{30}$$

The feedback gains are chosen such that the eigenvalues of the closed-loop matrix A_{cl}, match the desired closed-loop poles of the system

$$\det(pI - A_{cl}) = 0 \tag{31}$$

for $p = a_{d1}, a_{d2}, a_{d3}, a_{d4}$.

As the poles are functions of the complex feedback gains K_p, K_i, K_r, and K_c, the following equation can be derived from equation (31):

$$k = W^{-1}Z \tag{32}$$

where W is the coefficient matrix of the complex feedback gains obtained from $\det(pI - A_{cl})$ and Z is a vector of the closed-loop poles and system parameters. W and Z are presented in Appendix I. The solution of equation (32) provides the necessary gains to move the poles of the open-loop system to desired locations in the LHP.

B. LQR controller

The complex gains of the control law in (25) can also be obtained by using the Linear-Quadratic Regulator (LQR) theory. The objective of this controller is to obtain an optimal gain matrix, k, such that the closed-loop matrix, A_{cl}, is stable if the system is stabilizable. The A and B matrices of the open-loop state-space system of equation (28) are used in the design of the LQR controller. Although the LQR design is typically applied with real matrices, the theory and the algorithm implemented in MATLAB permit complex A and B matrices. In the implementation, the Q and R matrices were defined such that the state corresponding to the integrator had a larger gain and was moved further into the left half-plane. The following Q and R matrices were used in the design of the LQR controller:

$$Q = \begin{bmatrix} 1 & 0 & 0 & 0 \\ 0 & 1 & 0 & 0 \\ 0 & 0 & 10000 & 0 \\ 0 & 0 & 0 & 1 \end{bmatrix}, R = 2$$

IX. TEST-BED

The lab test bench includes the components of Fig. 1. This model is comparable to the IEEE first benchmark model for SSR studies [26] and was implemented with the following elements: Motorsolver DFIG generator and DC motor as a prime mover, dSPACE I/O box connected to dSPACE 1104 board in a PC host, Hirel Power Electronics Drive Board (PEDB), Grid Connection Box (with transformer, relay, and voltage sensing network), Current Sensor Board, Inductors (3), and AC Capacitors (3). The RSC is implemented through the PEDB and injects or absorbs power to/from the rotor through a 3-leg inverter under the control of the dSPACE board. The inductors represent the inductance of the transmission line as well as the transformer connecting the DFIG to the grid, and the capacitors represent the capacitors placed in series with the transmission line to compensate for the reactance of the line and transformers. The proposed control schemes used in the experiments are built in MATLAB/SIMULINK with embedded RTI1104 real-time interface for running the models on the dSPACE hardware.

Although the mechanical dynamics of the experimental system do not emulate a specific wind turbine, the mechanical system is not involved in a significant manner in the type of SSR studied in this paper. The resonances are mostly an electrical phenomenon [12], created by the interaction between the converter controllers and the series-compensated line. The DC motor with constant voltage imposes a speed that remains mostly constant at the time scales of the resonance, similar to

the behavior of a wind turbine with large inertia.

The lab test-bed also has parameter values that are different from a large-scale system (the estimated parameters of the test-bed are given in Appendix II). However, the differential equations describing the system are the same, and observations made on the small-scale system are useful to understand problems encountered in the larger system. Solutions can also be developed without risks or high costs, and with many of the real-world effects that limit the achievable performance in practice. Finally, although a single machine is considered, it has been argued that the collective behavior of a wind farm can be represented by an equivalent lumped machine in [27]-[29].

X. EXPERIMENTAL RESULTS

To demonstrate the effectiveness of the proposed controllers in mitigating SSR, experiments were carried out on the laboratory test-bed. The desired active and reactive powers were set to 20 W and 10 VAR, respectively. Both controllers were tested for a 70% compensation level. The results of the experiments are shown in Figs. 8 to 9.

Root-locus plots are also included and show how the poles move from the open-loop to the closed-loop values when the feedback gains are multiplied by a gain ranging from 0 to 1.

In the design of the pole-placement controller, the desired poles of the closed-loop system were specified in consideration of the open-loop poles. This is illustrated in Fig. 8 (b), where the imaginary parts of the closed-loop poles are the same as the open-loop poles. However, the real parts are made more negative to increase damping. As can be seen from the root-locus plots, the proposed controllers move the integrator pole from the origin further into the LHP. The DFIG system pole that is closest to the $j\omega$-axis (approximately at -20 rad/s) is also moved somewhat into the LHP. The other DFIG system pole (at approximately -170 rad/s) is moved slightly in the LHP. The pole that is added due to the series capacitor (at approximately -60 rad/s) is only moved slightly to the left in the LHP. The experimental results demonstrate the effectiveness of the controllers in mitigating SSR oscillations.

Small magnitude oscillations are observed in the plots. Investigations revealed that their frequencies were harmonics of the slip frequency and were due to imperfections in the rotor construction of the small-scale generator used to conduct the experiments. These oscillations would be expected to be much smaller in a larger machine.

Overall, the DFIG control system suppresses the SSR in two ways:
1. by using a grid-aligned reference frame obtained without actual grid measurements
2. by applying a state feedback control with integral action that ensures a closed-loop response with good damping.

The importance of the first element was demonstrated in the preliminary experiments. The combination of the two was evaluated in the experiments of this section and is further analyzed using frequency-response computations. Fig. 10 shows the frequency responses of the open-loop and closed-loop systems using the representation in complex variables. With the grid orientation, a zero frequency in these plots

corresponds to 60 Hz operation. In the complex representation, a system is described by Bode plots for positive and negative frequencies that are not symmetric. A positive frequency corresponds to a rotation of the complex variables in the same direction as the grid, while a negative frequency corresponds to reverse rotation. Fig. 10 (b) shows a resonant peak of the open-loop system at -16 Hz (corresponding to an SSR at 44 Hz). This peak is much smaller than would be obtained with stator alignment but is still present due to the series-compensation line. The pole placement controller is effective in suppressing the peak and associated SSR, while the integrator ensures a DC gain of 1 (0 dB).
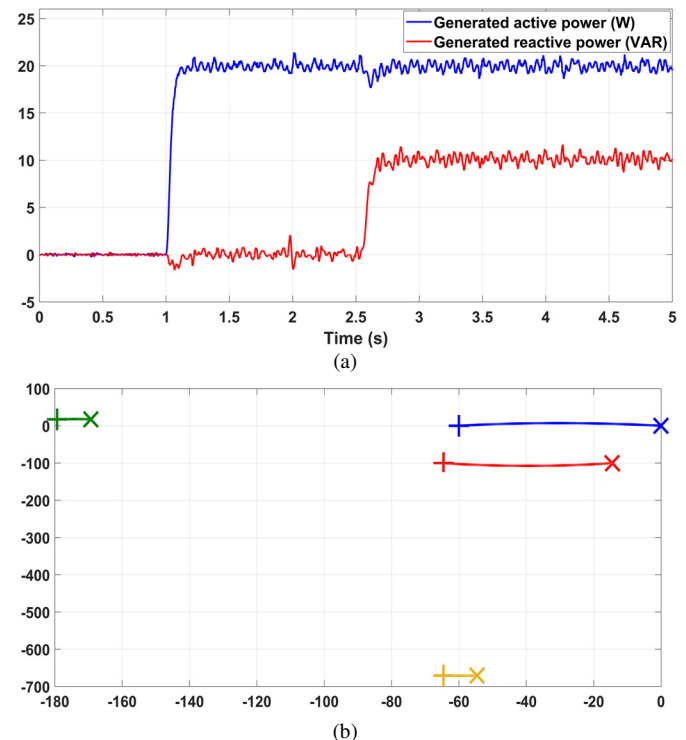
A. Pole-placement controller:

Fig. 8. Pole-placement controller for 70% compensation: (a) generated active and reactive powers, (b) root-locus of the system
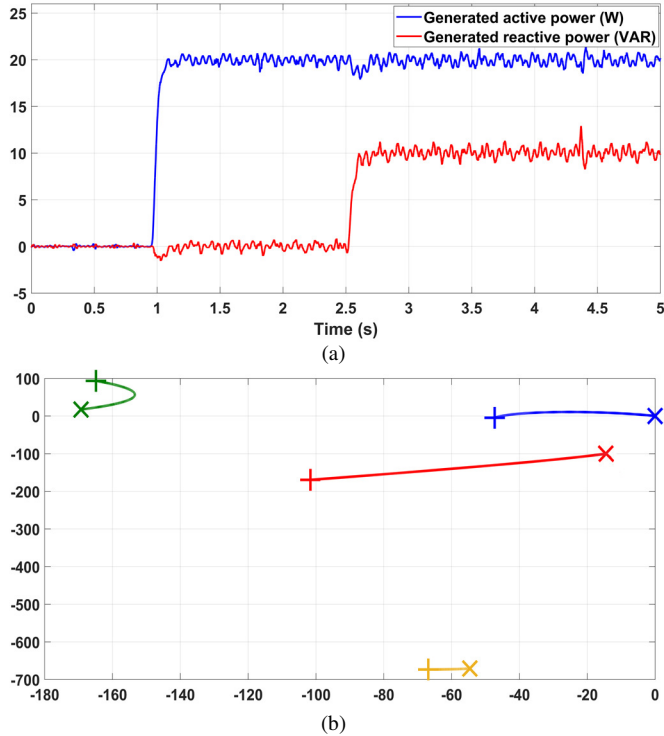
B. LQR controller:

Fig. 9. LQR controller for 70% compensation: (a) generated active and reactive powers, (b) root-locus of the system
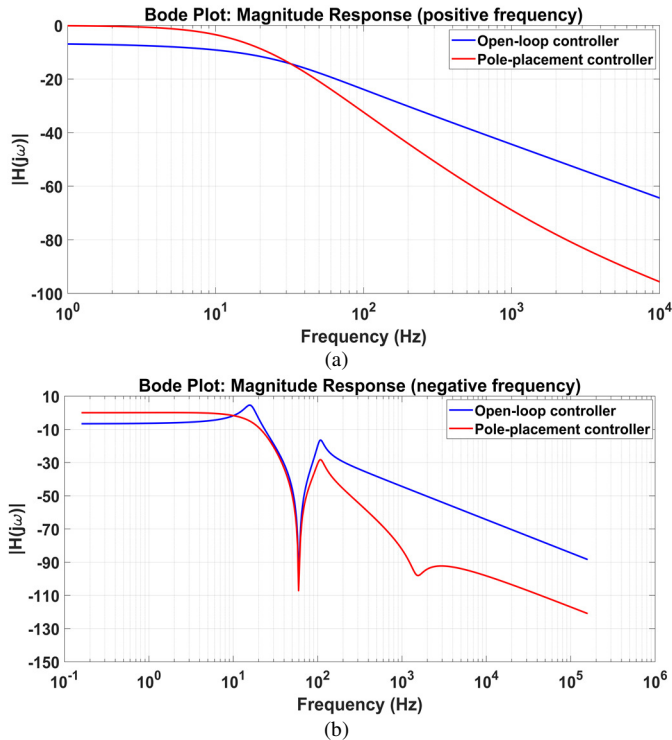

Fig. 10. The frequency response of the open-loop system and system with a pole-placement controller at 70% compensation

C. Effect of variable speed operation

The effectiveness of the proposed controllers in the presence of variable rotor speed is also studied through experiments on the laboratory test-bed. Steps of voltage are applied to the DC motor that is used as a prime mover. Over a period of 20 seconds, the slip changes from -30% to 30%. Both the pole-placement and the LQR controllers are effective at damping SSR oscillations in the generated active and reactive powers despite speed changes, as observed in Fig. 11.
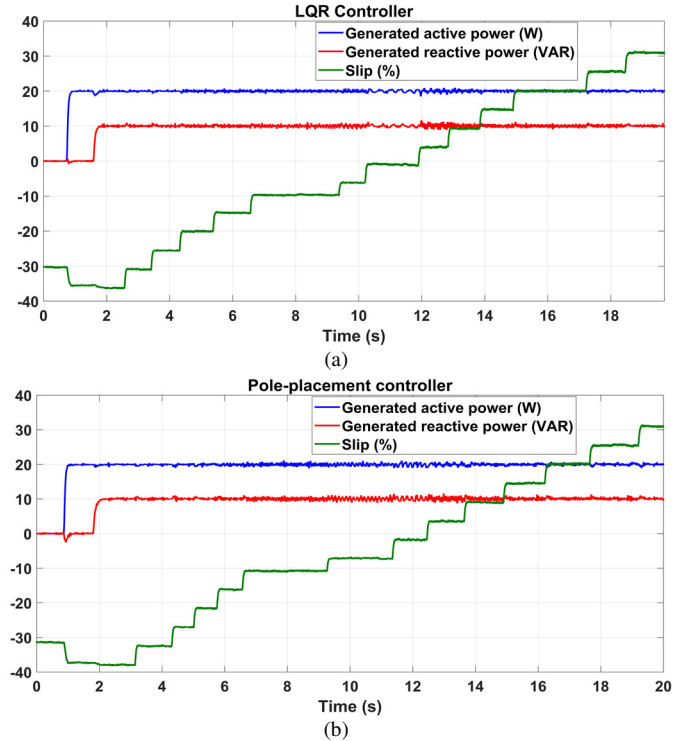

Fig. 11. Variable speed operation of the DFIG with 70% compensation: (a) LQR controller, (b) Pole-placement controller

XI. SIMULATION ON A LARGE-SCALE WIND FARM

The proposed scheme for mitigating SSR oscillations was also validated on a simulation of a wind farm comprised of 6 DFIGs, each rated at 1.5 MW. The wind farm is connected to the grid through step-up transformers and a 100 km line and is compensated at 70%.

The simulation that was used to evaluate the solution proposed in this paper originated from work done at the Institut de Recherche d'Hydro-Québec for modeling and simulating wind power plants for power system studies [30]. The turbine and drive train of this model are derived from [31]. The RSC of the original controller controls the speed and reactive power of the generator and aligns the d axis of the reference frame with the stator voltage.

The changes made to the original simulation are summarized below:

- The length of the transmission line in the simulation is increased from 30 km to 100 km so that, with 70% compensation, the total reactance remains the same as the uncompensated line in the original simulation. The objective is to set-up conditions where the steady-state operation is comparable without the series-compensated line and with the line. In particular, the active and reactive power levels and the stator and rotor currents remain about the same. The nominal controller

assuming direct grid connection can be used for comparison to the methods proposed in the paper.
- A series capacitor is added.
- The dq reference frame is aligned with the grid voltage.
- The RSC is replaced with the control scheme presented in section VIII without changing the PWM and voltage limiting elements.

This system is shown in Fig. 12 and its parameters are presented in Table II of Appendix I. All parameters are expressed in the per unit system with a base of 10 MVA.
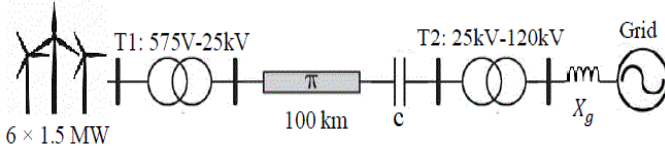

Fig. 12. The power system of the series-compensated DFIG based wind farm

Various components of the DFIG system, including the turbine, drive train, turbine controller, as well as the RSC and GSC controllers, are included in the simulation.

The pole-placement controller, combined with the alignment of the dq reference frame with the grid voltages, was found to effectively mitigate the SSR oscillations. This is illustrated in Fig. 13, where the response of the original system with and without the 70% series-compensated line (SC line), as well as the response using the proposed pole-placement controller in the presence of the SC line are observed. As can be seen from the figure, the response of the system with the scheme proposed in this paper is comparable to the response of the original controller without line compensation.

While other controllers in the literature (based on the design of auxiliary damping controllers) [14]-[16], [22] provide a damped response, results reported in the papers exhibit oscillations that decay over a period of several seconds. In contrast, the controllers presented in this paper produce a response without SSR oscillations and converging within the same time span as the system without the series-compensated line.
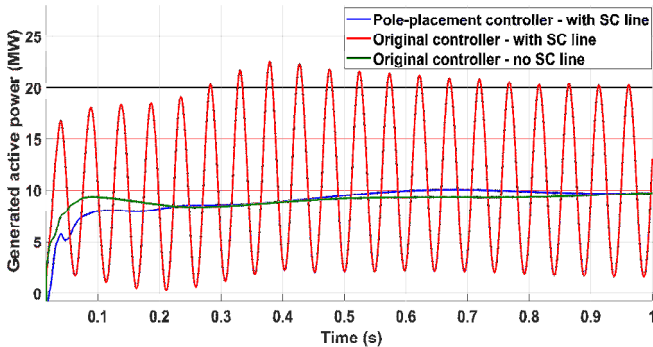

Fig. 13. Validation of the proposed scheme on a large-scale system in Simulink

XII. CONCLUSIONS

It would be risky and costly to perform experiments involving sub-synchronous resonances on a doubly-fed induction generator connected to the grid through a series-compensated line. Such data is not available in the literature, and the performance of control methods was previously demonstrated using computations and simulations only. The claims of this paper are supported by experiments on a physical test-bed that exhibits the limitations of real-world systems, although at a much smaller scale. The successful results from the lab scale experiments were further validated on a large-scale system in MATLAB/Simscape.

A main contribution of the paper was to show that the SSR problem in a DFIG connected to a series-compensated line is magnified when a stator alignment is used. Much trouble is therefore avoided by designing an observer that emulates a grid-alignment without requiring grid voltage measurements. A novel two-step approach was proposed for this purpose. What remained of the resonant behavior of the system was then controlled by conventional state feedback design.

The results of the paper also showed that sub-synchronous resonances could be suppressed without special hardware or communication with the grid or a series-capacitor. The active and reactive powers produced were well regulated at constant and varying speeds, suppressing the effect of SSR. A complex domain analysis reduced the 8th order series-compensated DFIG system with integral compensation to a 4th order one. Computations in the frequency-domain were consistent with the results of the experiments.

XIII. APPENDIX I

$$W = \begin{bmatrix} -Mc & L_t c & 0 & 0 \\ -2jMc\omega_e & -Mc & R_t c + 2jL_t c\omega_e & -M \\ Mc\omega_e^2 & -2jMc\omega_e & 1 - L_t c\omega_e^2 + jR_t c\omega_e & -jM\omega_e \\ 0 & 0 & 0 & Mc\omega_e^2 \end{bmatrix}$$

$$Z = \begin{bmatrix} L_r c R_t - c(M^2 - L_t L_r)A_1 - 2jM^2 c\omega_e + L_t L_r c\omega_e \\ L_r + M^2 c\omega_e^2 - c(M^2 - L_t L_r)A_2 - L_t L_r c\omega_e^2 + jL_r R_t c\omega_e \\ c(M^2 - L_t L_r)A_3 \\ -c(M^2 - L_t L_r)A_4 \end{bmatrix}$$

where
$A_1 = a_{d1} + a_{d2} + a_{d3} + a_{d4}$
$A_2 = a_{d1}a_{d2} + a_{d4}(a_{d1} + a_{d2} + a_{d3}) + a_{d3}(a_{d1} + a_{d2})$
$A_3 = a_{d4}(a_{d1}a_{d2} + a_{d3}(a_{d1} + a_{d2})) + a_{d1}a_{d2}a_{d3}$
$A_4 = a_{d1}a_{d2}a_{d3}a_{d4}$

XIV. APPENDIX II

The following parameters were estimated for the experimental test-bed:

TABLE I
EXPERIMENTAL TEST-BED PARAMETERS

R_s	$0.96\,\Omega$	L_s	$0.0131\,H$	R_l	$1.7\,\Omega$
R_r	$1.04\,\Omega$	L_r	$0.0098\,H$	L_l	$0.022\,H$
M	$0.0097\,H$	n_p	2	$c\,(70\%)$	$418\mu F$

The following parameters were used for the simulation model:

TABLE II
SIMULATION POWER SYSTEM PARAMETERS

R_s	0.023	L_s	3.08	R_l	0.18
R_r	0.016	L_r	3.06	L_l	0.63
M	2.9	n_p	3	c (70%)	2
R_{T1}	0.0016	L_{T1}	0.048	X_g	0.023
R_{T2}	0.0011	L_{T2}	0.006		

where

R_{T1}, R_{T2}, L_{T1}, L_{T2}: resistance and leakage inductances of transformers 1 and 2, respectively

X_g: reactance of the grid

XV. REFERENCES

[1] P. Mutschler, and R. Hoffmann, "Comparison of Wind Turbines Regarding Their Energy Generation," *2002 IEEE 33rd Annual IEEE Power Electronics Specialists Conference*, vol. 1, Cairns, Australia, pp. 6–11, June 2002.

[2] E. Vittal, and A. Keane, "Identification of Critical Wind Farm Locations for Improved Stability and System Planning", *IEEE Trans. Power Syst.*, vol. 28, no. 3, pp. 2950 - 2958, August 2013.

[3] A. M. Howlader, N. Urasaki, and A. Y. Saber "Control Strategies for Wind-Farm-Based Smart Grid System", *IEEE Trans. Ind. Appl.* vol. 50, no. 5, pp. 3591 – 3601, October 2014.

[4] P. Zhou, Y. He, and D. Sun, "Improved Direct Power Control of a DFIG-Based Wind Turbine During Network Unbalance," *IEEE Trans. Power Electron.*, vol. 24, no. 11, pp. 2465 - 2474, November 2009.

[5] J. V. Lamy, P. Jaramillo, I. L. Azevedo, and R. Wiser, "Should We Build Wind Farms Close to Load or Invest in Transmission to Access Better Wind Resources in Remote Areas? A case study in the MISO region," *Elsevier Energy Policy*, vol. 96, pp. 341–350, September 2016.

[6] H. Liu, X. Xie, C. Zhang, Y. Li, H. Liu, and Y. Hu, "Quantitative SSR Analysis of Series-Compensated DFIG-Based Wind Farms Using Aggregated RLC Circuit Model," *IEEE Trans. Power Syst.*, vol. 32, no. 1, pp. 474 - 483, January 2017.

[7] IEEE Committee Report, "Terms, Definitions, and Symbols for Subsynchronous Resonance Oscillations," *IEEE Trans. Power App. Syst*, vol. 104, pp. 1326–1334, June 1985.

[8] Subsynchronous Resonance Working Group of the System Dynamic Performance Subcommittee, "Reader's Guide to Subsynchronous Resonance," *IEEE Trans. Power Syst.*, vol. 7, no. 1, pp. 150-157, February 1992.

[9] H. Ghasemi, G. B. Gharehpetian, S. A. Nabavi-Niaki, and J. Aghaei, "Overview of Subsynchronous Resonance Analysis and Control in Wind Turbines," *Elsevier Renewable and Sustainable Energy Reviews*, pp. 234–243, 2013.

[10] Y. Luo, T. Bi, T. Zhang, and Q. Yang, "Impact of Fault Clearing Time on Shaft Torque Amplification in Series Compensated System," *2008 Third international conference on Electric Utility Deregulation and Restructuring and Power Technologies*, April 2008, pp. 709-713.

[11] A. Ostadi, A. Yazdani, and R. K. Varma, "Modeling and Stability Analysis of a DFIG-Based Wind-Power Generator Interfaced with a Series-Compensated Line," *IEEE Trans. Power Del.*, vol. 24, no. 3, pp. 1504 - 1514, July 2009.

[12] L. Fan, R. Kavasseri, Z. L. Miao, and C. Zhu, "Modeling of DFIG-Based Wind Farms for SSR Analysis," *IEEE Trans. Power Del.*, vol. 25, no. 4, pp. 2073 - 2082, October 2010.

[13] L. Fan, C. Zhu, Z. Miao, and M. Hu, "Modal Analysis of a DFIG-Based Wind Farm Interfaced with a Series Compensated Network," *IEEE Trans. Energy Convers.*, vol. 26, no. 4, pp. 1010-1020, December 2011.

[14] L. Fan, and Z. Miao, "Mitigating SSR Using DFIG-Based Wind Generation," *IEEE Trans. Sustainable Energy*, vol. 3, no. 3, pp. 349-358, July 2012.

[15] H. A. Mohammadpour, and E. Santi, "SSR Damping Controller Design and Optimal Placement in Rotor-Side and Grid-Side Converters of Series-Compensated DFIG-Based Wind Farm," *IEEE Trans. Sustainable Energy*, vol. 6, no. 2, pp. 388-399, April 2015.

[16] A. E. Leon, and J. A. Solsona, "Sub-Synchronous Interaction Damping Control for DFIG Wind Turbines," *IEEE Trans. Power Syst.*, vol. 30, no. 1, pp. 419-428, January 2015.

[17] L. Piyasinghe, Z. Miao, J. Khazaei, and Lingling Fan, "Impedance Model-Based SSR Analysis for TCSC Compensated Type-3 Wind Energy Delivery Systems," *IEEE Trans. Sustainable Energy*, vol. 6, no. 1, pp. 1-1, January 2015.

[18] H. A. Mohammadpour, and E. Santi, "Modeling and Control of Gate-Controlled Series Capacitor Interfaced With a DFIG-Based Wind Farm," *IEEE Trans. Ind. Electron.*, vol. 62, no. 2, pp.1022-1033, February 2015.

[19] R. K. Varma, S. Auddy, and Y. Semsedini, "Mitigation of Subsynchronous Resonance in a Series-Compensated Wind Farm Using FACTS Controllers," *IEEE Trans. Power Del.*, vol. 23, no. 3, pp. 1645–1654, July 2008.

[20] M. S. El-Moursi, B. Bak-Jensen, and M. H. Abdel-Rahman, "Novel STATCOM Controller for Mitigating SSR and Damping Power System Oscillations in A Series Compensated Wind Park," *IEEE Trans. Power Electron.*, vol. 25, no. 2, pp. 429–441, February 2010.

[21] T. Sadamoto, A. Chakraborty, T. Ishizaki, and J. Imura, "Retrofit Control of Wind-Integrated Power Systems," *IEEE Trans. Power Syst.*, vol. 33, no. 3, pp. 2804 - 2815, May 2018.

[22] P. Huong, M. S. El Moursi, W. Xiao, and J. L. Kirtley, "Subsynchronous Resonance Mitigation for Series-Compensated DFIG-Based Wind Farm by Using Two-Degree-of-Freedom Control Strategy," *IEEE Trans. Power Syst.*, vol. 30, no. 3, pp. 1442 - 1454, May 2015.

[23] A. Dòria-Cerezo and M. Bodson, "Root Locus Rules for Polynomials with Complex Coefficients," *21st Mediterranean Conference on Control and Automation*, Chania, Crete, pp. 663 – 670, 2013.

[24] H. Baesmat, and M. Bodson, "Pole Placement Control for Doubly-Fed Induction Generators Using Compact Representations in Complex Variables," *IEEE Trans. Energy Convers.*, to appear.

[25] H. Baesmat, and M. Bodson, "Design of Pole Placement Controllers for Doubly-Fed Induction Generators in the Complex Domain," *2015 IEEE Power & Energy Society General Meeting,* Denver, CO, pp. 1-5, 2015.

[26] IEEE Committee, "Report First Benchmark Model for Computer Simulation of Subsynchronous Resonance," *IEEE Trans. Power Apparat. Syst.*, vol. 96, no. 5, pp. 1565–1672, September/October 1977.

[27] D. Suriyaarachchi, U. Annakkage, C. Karawita, and D. Jacobson, "A Procedure to Study Sub-Synchronous Interactions in Wind Integrated Power Systems," *IEEE Trans. Power Syst.*, vol. 28, no. 1, pp. 377–384, February 2013.

[28] Z. Miao, "Impedance-Model-Based SSR Analysis for Type 3 Wind Generator and Series-Compensated Network," *IEEE Trans. Energy Convers.*, vol. 27, no. 4, pp. 984–991, December 2012.

[29] B. Badrzadeh, M. Sahni, Y. Zhou, D. Muthumuni, and A. Gole, "General Methodology for Analysis of Sub-Synchronous Interaction in Wind Power Plants," *IEEE Trans. Power Syst.*, vol. 28, no. 2, pp. 1858–1869, May 2013.

[30] R. Gagnon, G. Turmel, C. Larose, J. G. Brochu, G. Sybille, and M. Fecteau, "Large-Scale Real-Time Simulation of Wind Power Plants into Hydro-Québec Power System," *9th International Workshop on Large-Scale Integration of Wind Power into Power Systems as well as on Transmission Networks for Offshore Wind Power Plants*, Québec, Canada, 2010.

[31] N. W. Miller, J. J. Sanchez-Gasca, W. W. Price, and R. W. Delmerico, "Dynamic Modeling of GE 1.5 and 3.6 MW Wind Turbine-Generators for Stability Simulations," *2003 IEEE Power Engineering Society General Meeting,* Toronto, Canada, pp. 1977-1983, 2003.

Hana Jannaty Baesmat (S'13) received the B.Sc. degree in Electronic Engineering and M.Sc. degree in Electrical Engineering from the University of Kurdistan, Kurdistan, Iran, in 2007 and 2010, respectively. Currently, she is a Ph.D. candidate at the Department of Electrical and Computer Engineering at the University of Utah, UT, USA, and a Principal Electrical Engineer at Rio Tinto Kennecott Copper, UT, USA.

Marc Bodson (F'06) received the Ingénieur Civil Mécanicien et Electricien degree from the Université Libre de Bruxelles, Brussels, Belgium, in 1980, two M.S. degrees, one in electrical engineering and computer science and one in aeronautics and astronautics, from the Massachusetts Institute of Technology, Cambridge, MA, USA, in 1982, and the Ph.D. degree in electrical engineering and computer science from the University of California at Berkeley, Berkeley, CA, USA, in 1986. Currently, he is a Professor of Electrical and Computer Engineering with the University of Utah, Salt Lake City, UT, USA. He was Chair of the Department of Electrical and Computer Engineering from 2003 to 2009. Prof. Bodson was the Editor-in-Chief of the IEEE Transactions on Control Systems Technology from 2000 to 2003. He was elected Associate Fellow of the AIAA in 2013.